Hydrodynamic description of trapped ultracold paraexcitons in Cu_2O

S. Sobkowiak,* D. Semkat, and H. Stolz
Institut für Physik, Universität Rostock, 18051 Rostock, Germany
(Received 20 October 2014; revised manuscript received 23 January 2015; published 26 February 2015)

In this paper we present a theoretical model to describe the dynamics of paraexcitons in cuprous oxide at ultralow temperatures inside potential traps. A possible condensate is described by a generalized Gross-Pitaevskii equation. The noncondensed excitons evolve under a set of hydrodynamic equations, which were derived from a quantum Boltzmann equation. The model takes into account the finite lifetime of the excitons, the pump laser, the Auger-like two-body decay, as well as exciton-exciton and exciton-phonon scattering. The numerical results show the strong influence of the Auger effect on exciton temperatures and densities not only at high pump powers but also at ultralow temperatures. Furthermore, the excitons do not cool down to very low bath temperatures ($T_B \ll 0.5$ K) under continuous wave excitation. We also compare the results of the theoretical model with experimental data.

DOI: 10.1103/PhysRevB.91.075209 PACS number(s): 71.35.Lk, 63.20.kk, 67.85.Jk

I. INTRODUCTION

The experimental realization of an excitonic Bose-Einstein condensate (BEC) in a bulk material is a long standing problem. Initially put forward by Moskalenko [1] and Blatt *et al.* [2], the first experiments in excitonic systems were already carried out over 40 years ago [3]. Signatures of an excitonic BEC were first found using exciton-polaritons in microcavities [4–6]. Over the last decade experiments in these system have generated many interesting results and received a lot of attention (for an overview see [7]). Another intensively investigated system are indirect excitons in quantum wells [8–10], however, claims for an observation of an excitonic BEC are still under debate [11]. In bulk materials, despite many efforts from numerous research groups [12–16], no experiment so far has shown Bose-Einstein condensation of excitons demonstrating all the required criteria [17]. However, recent experimental results showed strong evidence for an excitonic condensate in cuprous oxide (Cu_2O) [18]. The long lifetime and the high binding energy of the excitons make this material a promising candidate for the realization of a BEC in a bulk material.

In typical experiments, excitons created by a pump laser are collected in stress induced potential traps. Using a ^{3}He/^{4}He dilution cryostate, the crystal specimen can be cooled to temperatures of the order of 100 mK [18,19]. The excitons in turn are cooled via interaction with the crystal lattice (phonons). Since excitons only have a finite lifetime and can undergo an Auger-like two-body decay, they might not reach the lattice temperature. Experimentally the exciton temperature is usually determined by fitting the decay luminescence spectrum with a Bose distribution. This spectral temperature T_S typically does not agree with the temperature of the helium bath T_B [16,18], hinting to a nonequilibrium state of the system. To understand this and other aspects of the recent experimental results, a theoretical model is needed. In order to identify a possible condensate in the experimental results, it is especially important to be able to differentiate between the features of a quasiequilibrium, a nonequilibrium, and a condensed case. Additionally, it would be beneficial to know the parameters for which the onset of condensation can be expected. In this paper we aim to develop such a theoretical model and thereby stimulating further progress in the field.

The situation in the experiments under consideration is quite complex. The theoretical model has to take into account the inhomogeneity of the system, the finite lifetime, a possible condensate, the Auger effect, exciton-exciton (X-X), and exciton-phonon (X-Ph) collisions. The semiconductor specific aspects (Auger effect, X-X, and X-Ph collisions) have already been investigated by different authors [20–22]. However, these papers only dealt with homogeneous systems. On the other hand, there is extensive literature on ultracold condensed atoms in potential traps. Excitons at the densities and temperatures present in typical experiments can be regarded as a gas of ultracold bosons. Therefore, extending the theory of ultracold atoms by taking into account semiconductor specific effects, should result in a model suitable for the description of trapped excitons in Cu_2O.

The paper is organized as follows: In the next section we discuss important features of the experiments under consideration. In the following two sections the theoretical model is developed and the implementation of the different processes is explained. In the last section typical numerical results are shown and first comparisons to experimental data are made.

II. EXPERIMENTAL BACKGROUND

The experiments in Refs. [16,18] investigate excitons consisting of a hole in the Γ_7^+ valence band and an electron in the Γ_6^+ conduction band (so-called yellow series). Since the valence and the conduction band both are doubly degenerate, the ground state of this series splits into the nondegenerate paraexciton and the triply degenerate orthoexciton. The different orthoexcitons are labeled according to their spin projection by (+), (0), and (−). Due to electron-hole exchange interaction, the paraexcitons are the energetically lowest state lying 12.12 meV below the orthoexcitons. The paraexcitons also have a long lifetime of $\tau = 650$ ns [16], making them the main focus of the experimental efforts. In the experiments presented in Refs. [16,18], the pump laser initially creates

*siegfried.sobkowiak@uni-rostock.de

orthoexcitons under involvement of a Γ_3^- phonon, outside of the trap center. These rapidly convert to paraexcitons via a phonon assisted process (reported rates are $\Gamma_{\text{O-P}} = 0.2\ \text{ns}^{-1}$ [23] and $\Gamma_{\text{O-P}} = 0.29\ \text{ns}^{-1}$ [22]). The potential trap created by the stress applied on the specimen is attractive for ortho(+), ortho(−), and paraexcitons, while being repulsive for ortho(0)excitons. The shape of the trap can be approximated by an isotropic harmonic oscillator potential with its minimum usually lying 1 to 3 meV below the band gap. The treatment of such an inhomogeneous three-component Bose gas is numerically quite cumbersome. As a first approximation we assume the ortho-para conversion to be almost instantaneous, taking only the paraexcitons directly into account in our model.

The excitation laser can be run in pulsed or continuous wave (cw) mode. Under cw excitation, new excitons are constantly created while others decay. After some time, both processes will balance out and the system will form a stationary, nonequilibrium state. However, under pulsed excitation, no new excitons will be created after the laser pulse. Therefore, after an initial nonequilibrium phase, the excitons will reach some kind of quasiequilibrium state. Their temperature, however, may still be different from the temperature of the crystal lattice.

III. MODEL

There are various approaches to theoretically describe ultracold atomic gases in nonequilibrium (for an overview see, e.g., Ref. [24]). The one most suitable for our purpose are the Zaremba-Nikuni-Griffin (ZNG) equations. Since these equations are well established in the literature, we will only briefly review the most important definitions and assumptions. A more detailed overview can be found in Ref. [25].

A. ZNG equations

In the ZNG equations, the system is split into a condensed and a noncondensed part by dividing the Bose-field operator $\hat{\psi}(\mathbf{r},t)$ into $\hat{\psi}(\mathbf{r},t) = \Phi(\mathbf{r},t) + \tilde{\psi}(\mathbf{r},t)$. The condensed phase is described by the condensate wave function $\Phi(\mathbf{r},t)$ and the noncondensed (thermal) phase by the fluctuation operator $\tilde{\psi}(\mathbf{r},t)$. The interaction of particles with each other is assumed to be well described by s-wave scattering with the interaction strength g.

The dynamics of the condensate is governed by a generalized Gross-Pitaevskii equation (GGPE)

$$i\hbar\frac{\partial\Phi(\mathbf{r},t)}{\partial t} = \Big[-\frac{\hbar^2\nabla^2}{2m} + V_{\text{ext}}(\mathbf{r}) + gn_c(\mathbf{r},t) + 2g\tilde{n}(\mathbf{r},t) - iR(\mathbf{r},t)\Big]\Phi(\mathbf{r},t), \tag{1}$$

with the condensate density $n_c(\mathbf{r},t) = |\Phi(\mathbf{r},t)|^2$, the density of the thermal particles $\tilde{n}(\mathbf{r},t) = \langle\tilde{\psi}^\dagger(\mathbf{r},t)\tilde{\psi}(\mathbf{r},t)\rangle$, and the coupling term $R(\mathbf{r},t)$. The latter is responsible for transferring particles between the condensed and the noncondensed phase and will be discussed later. In order to derive Eq. (1), the anomalous densities $\tilde{m}(\mathbf{r},t) = \langle\tilde{\psi}(\mathbf{r},t)\tilde{\psi}(\mathbf{r},t)\rangle$ were neglected.

Using an amplitude and phase representation for the wave function given by $\Phi(\mathbf{r},t) = \sqrt{n_c(\mathbf{r},t)}e^{i\theta(\mathbf{r},t)}$, the condensate velocity $\mathbf{v}_c(\mathbf{r},t)$ and the local time-dependent condensate chemical potential $\mu_c(\mathbf{r},t)$ can be introduced via

$$\begin{aligned}\mathbf{v}_c(\mathbf{r},t) &= \frac{\hbar}{m}\nabla\theta(\mathbf{r},t)\,,\\ \mu_c(\mathbf{r},t) &= -\frac{\hbar^2\nabla^2\sqrt{n_c(\mathbf{r},t)}}{2m\sqrt{n_c(\mathbf{r},t)}} + V_{\text{ext}}(\mathbf{r})\\ &\quad + gn_c(\mathbf{r},t) + 2g\tilde{n}(\mathbf{r},t).\end{aligned} \tag{2}$$

Using the above expressions, the energy of a particle in the condensate can be written as

$$\varepsilon_c(\mathbf{r},t) = -\hbar\frac{\partial\theta(\mathbf{r},t)}{\partial t} = \frac{1}{2}m\mathbf{v}_c^2(\mathbf{r},t) + \mu_c(\mathbf{r},t). \tag{3}$$

It should be noted that, to describe the condensate, Griffin *et al.* [25] used two coupled equations for $n_c(\mathbf{r},t)$ and $\mathbf{v}_c(\mathbf{r},t)$, which are equivalent to the GGPE (1).

The evolution of the thermal particles is described by the equation of motion for the fluctuation operator $\tilde{\psi}(\mathbf{r},t)$. Under the assumption of a slowly varying mean-field potential $U(\mathbf{r},t) = V_{\text{ext}}(\mathbf{r}) + 2g[n_c(\mathbf{r},t) + \tilde{n}(\mathbf{r},t)]$, it is possible to transform the equation of motion for $\tilde{\psi}(\mathbf{r},t)$ into a quantum Boltzmann equation for the Wigner distribution function $f(\mathbf{p},\mathbf{r},t)$. The result is given by

$$\frac{\partial f(\mathbf{p},\mathbf{r},t)}{\partial t} + \frac{\mathbf{p}}{m}\cdot\nabla_{\mathbf{r}}f(\mathbf{p},\mathbf{r},t) - \nabla_{\mathbf{r}}U(\mathbf{r},t)\cdot\nabla_{\mathbf{p}}f(\mathbf{p},\mathbf{r},t) = \left.\frac{\partial f(\mathbf{p},\mathbf{r},t)}{\partial t}\right|_{\text{coll.}}. \tag{4}$$

Using the first three moments of this equation, Griffin *et al.* [26] also derived a set of hydrodynamic equations describing the noncondensed particles. In the original ZNG formalism, the collision term on the right-hand side of Eq. (4) contains particle-particle collisions only. Collisions involving just thermal states are described by $C_{\text{X-X}}$, while $C_{\text{X}_c\text{-X}}$ contains collisions involving condensed and noncondensed states. The latter term transfers particles into or out of the condensate and is, therefore, related to the term $R(\mathbf{r},t)$ in the GGPE (1).

In the ZNG equations, the energy dispersion for the noncondensed particles is Hartree-Fock-like and, therefore, given by $\varepsilon_{\mathbf{p}}(\mathbf{r},t) = p^2/2m + U(\mathbf{r},t)$. The corresponding results using a Bogoliubov quasiparticle spectrum can be found in [27]. Since for typical experimental parameters only small or no condensates are expected, the Hartree-Fock-like dispersion is a good approximation.

B. Extensions

In order to include semiconductor specific effects, the collision term is extended to

$$\left.\frac{\partial f(\mathbf{p},\mathbf{r},t)}{\partial t}\right|_{\text{coll.}} = C_{\text{X-X}} + C_{\text{X}_c\text{-X}} + C_{\text{Ph}} + C_{\text{C-D}}, \tag{5}$$

where C_{Ph} describes X-Ph collisions and $C_{\text{C-D}}$ stands for processes that can create or destroy excitons. The latter namely includes the influence of the finite lifetime C_τ, the pump laser C_{laser}, and the Auger effect C_{Auger}. The X-Ph collision term has two contributions given by $C_{\text{Ph}} = C_{\text{X-Ph}} + C_{\text{X}_c\text{-Ph}}$. The term $C_{\text{X-Ph}}$ stands for X-Ph scattering within the thermal phase, while $C_{\text{X}_c\text{-Ph}}$ represents scattering of excitons into or out of the

condensate by phonons. In order to stay consistent with the GGPE (1) the coupling term $R(\mathbf{r},t)$ also needs to be extended with corresponding terms. This and the explicit form of the collision terms will be discussed in the next section.

The full numerical solution of the quantum Boltzmann equation (4) with the collision terms given by Eq. (5) is a challenging task. As we will discuss in the following, for the experiments under consideration it is beneficial to rewrite the Boltzmann equation (4) into a set of hydrodynamic equations. These are derived by multiplying Eq. (4) with ($\varphi_0 = 1, \varphi_1 = \mathbf{p}$, $\varphi_2 = p^2/2m$) and integrating over the whole momentum space [25]. This results in a set of three coupled equations for the density, momentum density, and kinetic energy density of the thermal excitons. The quantities are given by

$$\begin{aligned}\tilde{n}(\mathbf{r},t) &= \int \frac{d\mathbf{p}}{(2\pi\hbar)^3} f(\mathbf{p},\mathbf{r},t),\\ m\tilde{n}(\mathbf{r},t)\mathbf{v}_n(\mathbf{r},t) &= \int \frac{d\mathbf{p}}{(2\pi\hbar)^3}\mathbf{p} f(\mathbf{p},\mathbf{r},t),\\ E(\mathbf{r},t) &= \int \frac{d\mathbf{p}}{(2\pi\hbar)^3}\frac{p^2}{2m} f(\mathbf{p},\mathbf{r},t),\end{aligned} \tag{6}$$

where we have introduced the (normal) velocity $\mathbf{v}_n(\mathbf{r},t)$ of the noncondensed excitons.

Collision processes that conserve one or several of these quantities will not appear in the corresponding hydrodynamic equation. Since the X-X collision term $C_{\text{X-X}}$ conserves particle number, momentum, and kinetic energy, it will not appear at all. Therefore, the numerically demanding calculation of $C_{\text{X-X}}$ will not be necessary for evaluating the hydrodynamic equations.

Besides being coupled to each other, the resulting hydrodynamic equations will also be connected to the GGPE (1) by the moments of different collision terms. Additionally, they are in general not closed since the next higher moment will appear in the equation for the energy. One possible way of closing the equations is to assume a partial local equilibrium for the distribution function $f(\mathbf{p},\mathbf{r},t) = \tilde{f}_{\mathbf{p}}(\mathbf{r},t)$ given by

$$\begin{aligned}\tilde{f}_{\mathbf{p}}(\mathbf{r},t) &= [e^{[(\mathbf{p}-m\mathbf{v}_n)^2/2m+U-\tilde{\mu}(\mathbf{r},t)]/k_{\text{B}}T(\mathbf{r},t)} - 1]^{-1}\\ &= [e^{[\tilde{p}^2/2m-\tilde{\mu}_{\text{eff}}(\mathbf{r},t)]/k_{\text{B}}T(\mathbf{r},t)} - 1]^{-1}.\end{aligned} \tag{7}$$

Here k_{B} is Boltzmann's constant and $T(\mathbf{r},t)$ and $\tilde{\mu}(\mathbf{r},t)$ are the space- and time-dependent temperature and chemical potential. Rewriting the distribution function using the shifted momentum $\tilde{\mathbf{p}} = \mathbf{p} - m\mathbf{v}_n$ and the effective chemical potential $\tilde{\mu}_{\text{eff}}(\mathbf{r},t) = \tilde{\mu}(\mathbf{r},t) - U(\mathbf{r},t)$ recovers the simple form of a Bose distribution. The vanishing of the effective chemical potential [$\tilde{\mu}_{\text{eff}}(\mathbf{r},t) \to 0$] marks the onset of a possible condensate.

As we have shown in Ref. [28], the X-X and X-Ph collisions force the momentum distribution function into partial local equilibrium in less than 1 ns for the experimentally relevant parameters. On the other hand, the lifetime of the excitons and the time scales relevant for the drift into the trap center and the thermalization are usually of the order of several 100 ns. Due to this separation of time scales, the assumption of partial local equilibrium is justified after the initial stage of relaxation. The relaxation into partial local equilibrium, however, has to be treated separately.

The trap potential is well approximated by an isotropic harmonic oscillator potential [$V_{\text{ext}}(r) = \alpha r^2$]. Therefore, for our calculations we use spherical symmetry. Even though this does not match the excitation geometry exactly, the impact on the physical quantities in the trap center should be limited since the excitation region is far away from it. The result for the hydrodynamic equations in quasi-one-dimension is

$$\begin{aligned}&\frac{\partial\tilde{n}}{\partial t} + \frac{\partial}{\partial r}[\tilde{n}v_n]\\ &\quad= \Gamma^{(0)}_{\text{X}_\text{c}\text{-X}} + \Gamma^{(0)}_{\text{X}_\text{c}\text{-Ph}} + \Gamma^{(0)}_{\text{C-D}} - \frac{2}{r}\tilde{n}v_n,\\ &\frac{\partial}{\partial t}[m\tilde{n}v_n] + \frac{\partial}{\partial r}[m\tilde{n}v_n^2 + \tilde{P}]\\ &\quad= -\tilde{n}\frac{\partial U}{\partial r} - \frac{2}{r}m\tilde{n}v_n^2 + mv_c\Gamma^{(0)}_{\text{X}_\text{c}\text{-X}} + \Gamma^{(1)}_{\text{X-Ph}} + \Gamma^{(1)}_{\text{X}_\text{c}\text{-Ph}} + \Gamma^{(1)}_{\text{C-D}},\\ &\frac{\partial E}{\partial t} + \frac{\partial}{\partial r}[(E+\tilde{P})v_n]\\ &\quad= -\tilde{n}v_n\frac{\partial U}{\partial r} + (\varepsilon_c - U)\Gamma^{(0)}_{\text{X}_\text{c}\text{-X}} - \frac{2}{r}(E+\tilde{P})v_n + \Gamma^{(2)}_{\text{X-Ph}}\\ &\qquad+ \Gamma^{(2)}_{\text{X}_\text{c}\text{-Ph}} + \Gamma^{(2)}_{\text{C-D}},\end{aligned} \tag{8}$$

where $\Gamma^{(n)}$ stands for the nth moment of the collision term C given by

$$\Gamma^{(n)} = \int \frac{d\mathbf{p}}{(2\pi\hbar)^3}\varphi_n(\mathbf{p})\, C. \tag{9}$$

The local kinetic pressure $\tilde{P}(\mathbf{r},t)$ is given by

$$\tilde{P}(\mathbf{r},t) = \frac{2}{3}\int \frac{d\mathbf{p}}{(2\pi\hbar)^3}\frac{(\mathbf{p}-m\mathbf{v}_n)^2}{2m}\tilde{f}_{\mathbf{p}}(\mathbf{r},t). \tag{10}$$

In order to solve this system of equations, the moments of the collision terms are needed. These are discussed in the following section.

IV. COLLISION TERMS

A. Exciton-exciton collisions ($C_{\text{X}_\text{c}\text{-X}}$)

The collision term $C_{\text{X}_\text{c}\text{-X}}$ describes collisions between two excitons which scatter an exciton into or out of the condensate. Therefore, it is responsible for exchanging excitons between the condensed and the noncondensed phase. In the hydrodynamic equations (8) only the zeroth moment of $C_{\text{X}_\text{c}\text{-X}}$ appears. Under the assumption of partial local equilibrium it is given by [25]

$$\begin{aligned}\Gamma^{(0)}_{\text{X}_\text{c}\text{-X}} = &-\frac{2g^2 n_c}{(2\pi)^5\hbar}(1 - e^{-[\tilde{\mu}-\mu_c-\frac{m}{2}(\mathbf{v}_n-\mathbf{v}_c)^2]/k_{\text{B}}T})\\ &\times\int d\mathbf{k}_1 d\mathbf{k}_2 d\mathbf{k}_3\,\delta(\mathbf{k}_c + \mathbf{k}_1 - \mathbf{k}_2 - \mathbf{k}_3)\\ &\times\delta\big(\varepsilon_c + \varepsilon_{\mathbf{k}_1} - \varepsilon_{\mathbf{k}_2} - \varepsilon_{\mathbf{k}_3}\big)\big(1 + \tilde{f}_{\mathbf{k}_1}\big)\tilde{f}_{\mathbf{k}_2}\tilde{f}_{\mathbf{k}_3},\end{aligned} \tag{11}$$

with $\mathbf{k}_c = m\mathbf{v}_c/\hbar$. The corresponding term for the GGPE (1) reads

$$R_{\text{X}_\text{c}\text{-X}}(\mathbf{r},t) = \frac{\hbar\Gamma^{(0)}_{\text{X}_\text{c}\text{-X}}}{2n_c(\mathbf{r},t)}. \tag{12}$$

B. Exciton-phonon collisions (C_{Ph})

In an unstrained crystal of Cu_2O, the yellow $1s$ paraexcitons can interact with longitudinal acoustic (LA), but not with transversal acoustic (TA) phonons. However, when stress is applied, as in the experiments under consideration, interaction with either type of phonons is possible. The collision term $C_{\text{X-Ph}}$ for both processes is given by [20]

$$\begin{aligned} C_{\text{X-Ph}} = -\frac{\pi D^2}{\varrho v_s}\int \frac{d\mathbf{k}'}{(2\pi)^3}|\mathbf{k}'-\mathbf{k}|\{&\big[f_{\mathbf{k}}\big(1+f^{\mathrm{Ph}}_{\mathbf{k}-\mathbf{k}'}\big)(1+f_{\mathbf{k}'}) \\ &-(1+f_{\mathbf{k}})f^{\mathrm{Ph}}_{\mathbf{k}-\mathbf{k}'}f_{\mathbf{k}'}\big]\delta(\varepsilon_{\mathbf{k}}-\varepsilon_{\mathbf{k}'}-\hbar\omega_{\mathbf{k}-\mathbf{k}'}) \\ &+\big[f_{\mathbf{k}}f^{\mathrm{Ph}}_{\mathbf{k}'-\mathbf{k}}(1+f_{\mathbf{k}'})-(1+f_{\mathbf{k}})\big(1+f^{\mathrm{Ph}}_{\mathbf{k}'-\mathbf{k}}\big)f_{\mathbf{k}'}\big] \\ &\times\delta(\varepsilon_{\mathbf{k}}-\varepsilon_{\mathbf{k}'}+\hbar\omega_{\mathbf{k}'-\mathbf{k}})\}, \end{aligned} \tag{13}$$

with the deformation potential D, the crystal density $\varrho = 6.11\times10^3\ \mathrm{kg/m^3}$ [20], and the speed of sound v_s. The first (second) term on the right-hand side represent Stokes (anti-Stokes) scattering, respectively. The phonons are assumed to be in equilibrium at the lattice temperature T_{Ph}, therefore, their distribution function is given by $f^{\mathrm{Ph}}_{\mathbf{k}'-\mathbf{k}} = [\exp(\hbar\omega_{\mathbf{k}'-\mathbf{k}}/k_BT_{\mathrm{Ph}})-1]^{-1}$ with the phonon energy $\hbar\omega_{\mathbf{k}'-\mathbf{k}} = \hbar v_s|\mathbf{k}'-\mathbf{k}|$.

Applying the integration over all $\mathbf{k}$ on $C_{\text{X-Ph}}$ to calculate the moments, allows the exchange of $\mathbf{k}$ and $\mathbf{k}'$ in the Stokes scattering term. This results in a very compact form for all moments

$$\begin{aligned} \Gamma^{(n)}_{\text{X-Ph}} = -\frac{\pi D^2}{\varrho v_s}\int \frac{d\mathbf{k}d\mathbf{k}'}{(2\pi)^6}|\mathbf{k}'-\mathbf{k}|[\varphi_n(\mathbf{k})-\varphi_n(\mathbf{k}')] \\ \times\big[f_{\mathbf{k}}f^{\mathrm{Ph}}_{\mathbf{k}'-\mathbf{k}}(1+f_{\mathbf{k}'})-(1+f_{\mathbf{k}})\big(1+f^{\mathrm{Ph}}_{\mathbf{k}'-\mathbf{k}}\big)f_{\mathbf{k}'}\big] \\ \times\delta(\varepsilon_{\mathbf{k}}-\varepsilon_{\mathbf{k}'}+\hbar\omega_{\mathbf{k}'-\mathbf{k}}). \end{aligned} \tag{14}$$

From Eq. (14) it follows directly that $\Gamma^{(0)}_{\text{X-Ph}}$ vanishes ($\varphi_0 = 1$).

The second X-Ph collision term $C_{\text{X}_c\text{-Ph}}$ can also be extracted from Ref. [20] and has already been given in Ref. [29]. Within our model its moments read

$$\begin{aligned} \Gamma^{(n)}_{\text{X}_c\text{-Ph}} = -\frac{\pi D^2 n_c}{\rho v_s}\int \frac{d\mathbf{k}}{(2\pi)^3}\varphi_n(\mathbf{k})|\mathbf{k}_c-\mathbf{k}|\{&\big[f_{\mathbf{k}}\big(1+f^{\mathrm{Ph}}_{\mathbf{k}-\mathbf{k}_c}\big) \\ &-(1+f_{\mathbf{k}})f^{\mathrm{Ph}}_{\mathbf{k}-\mathbf{k}_c}\big]\delta(\varepsilon_{\mathbf{k}}-\varepsilon_c-\hbar\omega_{\mathbf{k}-\mathbf{k}_c}) \\ &+\big[f_{\mathbf{k}}f^{\mathrm{Ph}}_{\mathbf{k}_c-\mathbf{k}}-(1+f_{\mathbf{k}})\big(1+f^{\mathrm{Ph}}_{\mathbf{k}_c-\mathbf{k}}\big)\big] \\ &\times\delta(\varepsilon_{\mathbf{k}}-\varepsilon_c+\hbar\omega_{\mathbf{k}_c-\mathbf{k}})\}. \end{aligned} \tag{15}$$

In the system under consideration the corresponding imaginary part of (15) is typically very small compared to the other dispersive shift terms in (1) and has been neglected. Therefore, the term for the GGPE (1) reads

$$R_{\text{X}_c\text{-Ph}}(\mathbf{r},t) = \frac{\hbar\Gamma^{(0)}_{\text{X}_c\text{-Ph}}}{2n_c(\mathbf{r},t)}. \tag{16}$$

The speeds of sound are given by $v_s^{\mathrm{LA}} = 4.5\times10^3$ m/s and $v_s^{\mathrm{TA}} = 1.3\times10^3$ m/s [30]. The deformation potential for the TA phonons depends on the applied stress and can be calculated using the method explained in Ref. [28]. In this paper we use the value $D^{\mathrm{TA}} = 0.235$ eV, which corresponds to a trap depth of around 2 meV. For the LA phonons we use the value $D^{\mathrm{LA}} = 1.68$ eV given by Ref. [31].

C. Lifetime (C_τ)

Since the decay of the excitons mainly originates from nonradiative transitions, the lifetime can be described by a constant τ. Its collision term is given by $C_\tau = -\tilde{f}_{\mathbf{p}}(\mathbf{r},t)/\tau$. Therefore, the calculation of the moments is straightforward and yields

$$\begin{aligned} \Gamma^{(0)}_\tau &= -\tilde{n}(\mathbf{r},t)/\tau, \\ \Gamma^{(1)}_\tau &= -m\tilde{n}(\mathbf{r},t)\mathbf{v}_n(\mathbf{r},t)/\tau, \\ \Gamma^{(2)}_\tau &= -E(\mathbf{r},t)/\tau. \end{aligned} \tag{17}$$

For our computations we used the value $\tau = 650$ ns [18]. We assume the same lifetime for the condensed excitons.

D. Pump laser (C_{laser})

In order to incorporate new excitons into the system of Eqs. (8), their relaxation into partial local equilibrium has to be treated first. We assume that the excitons created by the laser are at rest and do not gain any velocity during this initial relaxation. Therefore, we simulate the relaxation into partial local equilibrium by solving a homogeneous Boltzmann equation for an initial momentum distribution function at all relevant points in space. For this we take into account X-X and X-Ph scattering (see Ref. [28] for details). The initial energy of the excitons depends on the wavelength of the laser, the exchange splitting between ortho- and paraexcitons, and the energy of the phonon emitted during the conversion process. For the excitation scheme considered here the initial energy is about 8 meV. Therefore, the initial momentum distribution function is peaked at the corresponding $\mathbf{k}$ value and normalized to the density of the newly created excitons $n_{\mathrm{laser}}(\mathbf{r},t)$. Its value can be estimated from the pulse shape and the fraction of absorbed photons [16]. For our calculations we assume $n_{\mathrm{laser}}(\mathbf{r},t)$ to be a Gaussian distribution along r with its maximum at r_{max} outside the trap center and a width of σ. The normalization is chosen to reproduce the same rate of exciton generation as a laser with a given pump power P_{L} would create in actual experiments.

The relaxation into partial local equilibrium takes no more than 1 ns. The remaining exciton energy after this initial relaxation $E_{\mathrm{laser}}(\mathbf{r},t)$ typically corresponds to temperatures around 4 K. Since we assumed the excitons to be at rest during this time, the new excitons enter the hydrodynamic equations with density $n_{\mathrm{laser}}(\mathbf{r},t)$ and energy $E_{\mathrm{laser}}(\mathbf{r},t)$ but with $\Gamma^{(1)}_{\mathrm{laser}} = \mathbf{0}$. The moments of C_{laser} are (symbolically) given by

$$\begin{aligned} \Gamma^{(0)}_{\mathrm{laser}} &= n_{\mathrm{laser}}(\mathbf{r},t), \\ \Gamma^{(1)}_{\mathrm{laser}} &= \mathbf{0}, \\ \Gamma^{(2)}_{\mathrm{laser}} &= E_{\mathrm{laser}}(\mathbf{r},t). \end{aligned} \tag{18}$$

E. Auger effect (C_{Auger})

The Auger-like two-body decay destroys two excitons, recombining one and ionizing the other. The resulting electron-hole pair can rebind to form a high energy exciton. The transition matrix elements of the dominant terms for the Auger effect are linear in $\mathbf{k}$ [32]. Note that this means that the condensed excitons should not undergo an Auger-like decay.

For the thermal excitons we use a **k**-averaged Auger rate A as found in experiments [16,33,34]. The destruction of excitons due to the Auger effect can then be described by the collision term $C^{\mathrm{D}}_{\mathrm{Auger}} = -2A\tilde{n}(\mathbf{r},t)\tilde{f}_{\mathbf{p}}(\mathbf{r},t)$ [22]. The calculation of the moments for this term is straightforward.

For our model we assume that all electron-hole pairs rebind and that the newly formed excitons are equally distributed over the four possible exciton states (one para- and three orthoexcitons). Since ortho(0) excitons are expelled from the trap, they will not be refed into Eqs. (8). The newly formed excitons are assumed to be at rest. Their energy is equivalent to the binding energy of 150 meV. Therefore, they can emit different optical phonons. Taking this into account, we calculate their energy after the relaxation into partial local equilibrium (E_{Auger}) the same way we did for the excitons created by the pump laser (by solving a homogeneous Boltzmann equation). The moments are given by

$$\begin{aligned}\Gamma^{(0)}_{\mathrm{Auger}} &= -2A\tilde{n}^2(\mathbf{r},t) + \frac{3}{4}A\tilde{n}^2(\mathbf{r},t),\\ \Gamma^{(1)}_{\mathrm{Auger}} &= -2Am\tilde{n}^2(\mathbf{r},t)\mathbf{v}_n(\mathbf{r},t),\\ \Gamma^{(2)}_{\mathrm{Auger}} &= -2A\tilde{n}(\mathbf{r},t)E(\mathbf{r},t) + \frac{3}{4}A\tilde{n}(\mathbf{r},t)E_{\mathrm{Auger}}.\end{aligned} \tag{19}$$

The value of the Auger rate A has been determined theoretically and experimentally. However, the results vary over several orders of magnitude. The theoretical calculations predict $A = 2\times10^{-21}$ cm^3 ns^{-1} [35] and $A = 3\times10^{-22}$ cm^3 ns^{-1} [32] while the values $A = 2\times10^{-18}$ cm^3 ns^{-1} [18], $A = 7\times10^{-17}$ cm^3 ns^{-1} [33], and $A = 4\times10^{-16}$ cm^3 ns^{-1} [34] were found experimentally. Therefore, the Auger rate A is a source of uncertainty.

F. Summary of the model

The model consists of a GGPE (1) describing the condensed excitons coupled to a set of hydrodynamic equations (8) for the noncondensed excitons. The coupling term $R(\mathbf{r},t)$ in (1) reads

$$R(\mathbf{r},t) = R_{\mathrm{X_c\text{-}X}}(\mathbf{r},t) + R_{\mathrm{X_c\text{-}Ph}}(\mathbf{r},t) + \hbar/\tau. \tag{20}$$

The distribution function for the thermal excitons is given by (7). The initial relaxation into this partial local equilibrium is treated separately. For our numerical calculations we usually start with thermal excitons only. Monitoring the effective chemical potential the condensate is seeded into the system if necessary.

Comparable approaches using a GGPE coupled to a quantum Boltzmann or hydrodynamic equations are also used to describe exciton-polaritons in microcavities [29,36].

V. RESULTS

For the calculations we choose parameters comparable to the values found in Refs. [16,18]. The laser is placed 100 μm outside of the trap center ($r_{\max} = 100\ \mu$m) with a width of $\sigma = 3\ \mu$m. For the interaction strength g we use $g = 4\pi\hbar^2 a_s/m = 0.54$ eV nm^3, which corresponds to a s-wave scattering length of $a_s = 2.1\,a_B$ [37], a Bohr radius of $a_B = 0.7$ nm, and an exciton mass of [38] $m = 2.6\,m_0$ (m_0: free electron mass). For the discussion it is useful to review the different temperatures present in our theoretical model. There is the temperature of the helium bath T_{B} and the temperature of the phonons (of the crystal lattice) T_{Ph}. For our calculations we assume $T_{\mathrm{Ph}} = T_{\mathrm{B}}$. Additionally, there is the temperature of the excitons, which will be depending on space and time $T(r,t)$. We will further introduce the exciton temperature in the trap center $T_0 = T(r=0,t)$ and the mean exciton temperature

$$\langle T\rangle = \frac{1}{N}\int d\mathbf{r}\,T(r,t)\tilde{n}(r,t) \tag{21}$$

which both depend on time only. The temperature extracted from fitting the experimental spectra will be called the spectral temperature T_{S}. In the following we will present some general results for cw excitation and discuss different features before comparing theoretical results with experimental data.

A. General results

For the calculations in this section, the trap parameter α was set to $\alpha = 0.11\ \mu$eV μm^{-2}. Figure 1 shows results for a moderate pumping power of $P_{\mathrm{L}} = 26.4\ \mu$W and a phonon temperature of $T_{\mathrm{Ph}} = 0.5$ K. As can be seen very well, the stationary state of the system shows strong deviations from the corresponding equilibrium situation. The density profile is similar to a Gaussian shape, with an increased value at the trap center. The shape of the other quantities is due to the constant creation of excitons by the pump laser at $r = 100\ \mu$m. The newly created "hot" excitons drift towards the center of the trap. At first their velocity increases strongly, slows down afterwards, and is zero in the central region of the trap. During the drift process, the excitons are cooled via phonon interaction. The temperature drops progressively, reaching a minimum of $T_{\min} = 0.54$ K around $r = 20\ \mu$m. As of this point, the temperature rises slightly reaching a local maximum of $T_0 = 0.55$ K at $r = 0$ due to the Auger effect. The effective chemical potential behaves inversely. However, it increases

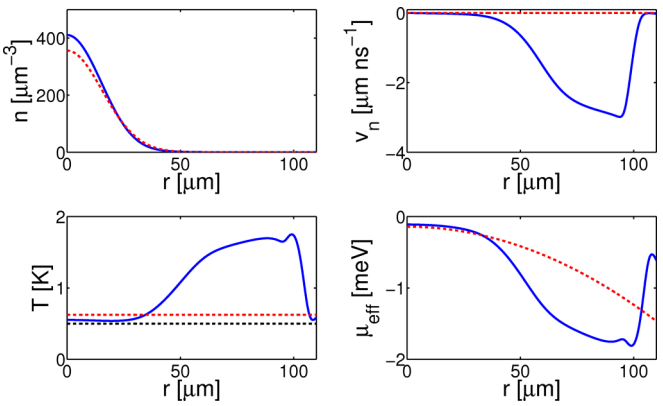

FIG. 1. (Color online) Density $\tilde{n}(r)$, velocity $v_n(r)$, temperature $T(r)$, and effective chemical potential $\tilde{\mu}_{\mathrm{eff}}(r)$ for the stationary state (blue solid line) at a phonon temperature of $T_{\mathrm{Ph}} = 0.5$ K and a laser power of $P_{\mathrm{L}} = 26.4\ \mu$W. The dashed red curves represent the corresponding values of a distribution function in equilibrium with the same mean temperature $\langle T\rangle = 0.62$ K and the same exciton number $N = 2.13\times10^7$. The dashed black curve shows the phonon temperature T_{Ph}. The Auger rate is set to $A = 2.0\times10^{-18}$ cm^3/ns.

steadily towards the trap center. The results shown in Fig. 1 are typical for cw excitation. The curves for the outer region of the trap ($r > 60\ \mu$m) do not differ qualitatively for other parameters. Therefore, we will concentrate on the inner region of the trap for the following results.

For the experimental realization of an excitonic condensate, one has to create high densities at low temperatures. Since the Auger effect scales quadratically with the density, it seems favorable to use low pump powers at ultralow temperatures in order to minimize its influence. The results for $P_L = 2.8\ \mu$W and different phonon temperatures are shown in Fig. 2. The total number of excitons varies only weakly between $N = 2.74 \times 10^6$ ($T_{Ph} = 1.0$ K) and $N = 2.57 \times 10^6$ ($T_{Ph} = 0.037$ K). Since the extension of the thermal cloud shrinks with decreasing temperatures, the density in the trap center has to increase accordingly. Therefore, lowering the phonon temperature at a constant pump power actually increases the influence of the Auger effect. The temperature curves illustrate this well. For the cases $T_{Ph} = 1.0$ K and $T_{Ph} = 0.5$ K, the exciton temperatures in the trap center are very close to the respective phonon temperatures. The monotonous course of the curves clearly indicates a very weak influence of the Auger effect. In case of the ultralow phonon temperature of $T_{Ph} = 0.037$ K, the temperature forms the typical shape for a strong influence of the Auger effect (minimum outside the trap center and a local maximum at $r = 0$). The temperature in the trap center is $T_0 = 0.25$ K and hence well above the phonon temperature. The mean temperature $\langle T \rangle = 0.38$ K is even one order of magnitude higher than the phonon temperature. This clearly illustrates the crucial role of the Auger effect, which becomes increasingly important not only at high pump powers but also at ultralow temperatures. However, there is another important effect at ultralow temperatures, the finite thermalization time. Due to the "freezing out" of phonons [20], the thermalization time becomes increasingly longer at lower and lower bath temperatures. Setting $A = 0$ results in the dashed-dotted black temperature curve in Fig. 2. The exciton

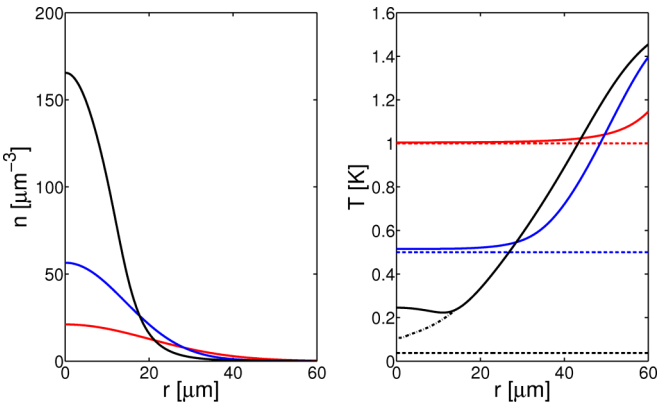

FIG. 2. (Color online) Density $\tilde{n}(r)$ and temperature $T(r)$ for the stationary state at a laser power of $P_L = 2.8\ \mu$W, a phonon temperature of $T_{Ph} = 1.0$ K (solid red curve), $T_{Ph} = 0.5$ K (solid blue curve), and $T_{Ph} = 0.037$ K (solid black curve), and an Auger rate of $A = 2.0 \times 10^{-18}$ cm^3/ns. The dashed lines of the same color show the respective phonon temperatures. The dash-dotted black line in the right panel shows the temperature for $T_B = 0.037$ K and $A = 0$.

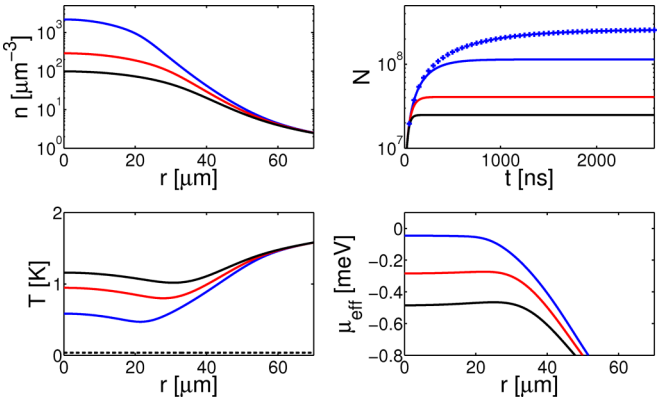

FIG. 3. (Color online) Density $\tilde{n}(r)$, temperature $T(r)$, and effective chemical potential $\tilde{\mu}_{eff}(r)$ for the stationary state at a phonon temperature of $T_{Ph} = 0.037$ K and a laser power of $P_L = 262\ \mu$W as well as the evolution of the total exciton number $N(t)$. The Auger rates are $A = 2.0 \times 10^{-18}$ cm^3/ns [18] (blue curves), $A = 7.0 \times 10^{-17}$ cm^3/ns [33] (red curves), and $A = 4.0 \times 10^{-16}$ cm^3/ns [34] (black curves). The blue crosses mark the development of the exciton number without the Auger effect. The black dashed line represents the phonon temperature.

temperature is monotonously dropping towards the trap center, however, it never reaches the actual bath temperature. This is due to the finite lifetime of the excitons which in this case is too short for a complete thermalization. Hence, even if the Auger effect could be "turned off" in the actual experiments, one can still not expect the excitons to be fully thermalized with the lattice at ultralow bath temperatures. However, in most experimentally relevant cases, the influence of the Auger effect will be dominant compared to the finite thermalization time. Therefore, the uncertainty associated with the Auger rate A is problematic for any predictions of the onset of a BEC of excitons.

How the Auger rate affects the different quantities is shown in Fig. 3. The results were obtained by using three different Auger rates from the literature and keeping all other parameters (phonon temperature, pump power, ...) constant. Important values for the different curves in Fig. 3 are listed in Table I. While the shape of the density profiles stay qualitatively the same, the quantitative value in the trap center changes by more than one order of magnitude between the smallest and the largest Auger rate. Accordingly, the exciton number in the stationary state changes by more than a factor of four between these cases. The temperature curves all display the typical form indicating a strong influence of the Auger effect. The temperature in the trap center and the mean temperature for $A = 2.0 \times 10^{-18}$ cm^3/ns and $A = 4.0 \times 10^{-16}$ cm^3/ns

TABLE I. Key values in the stationary state for the results shown in Fig. 3.

A (cm^3/ns)	$N/10^8$	$\langle T \rangle$ (K)	T_0 (K)	T_{min} (K)	$\tilde{n}_0$ (μm^{-3})
2×10^{-18}	1.14	0.65	0.58	0.47	2175.6
7×10^{-17}	0.41	1.03	0.95	0.80	288.9
4×10^{-16}	0.25	1.24	1.16	1.02	98.2

differ by approximately a factor of two. Due to the strong heating introduced by the Auger effect, the maximum of the effective chemical potential for $A = 4.0 \times 10^{-16}$ cm^3/ns and $A = 7.0 \times 10^{-17}$ cm^3/ns does not even lie in the center of the trap. For these high Auger rates, there will probably be no onset of a BEC within our model.

B. Comparison with experiments

In the following we compare theoretical results with the corresponding experimental data for two different situations.

The first set of examples is taken from Ref. [18]. In the experiment, cw excitation was used over a wide range of pumping powers for a helium bath temperature of $T_B = 0.037$ K. The experimentally determined Auger rate is $A = 2.0 \times 10^{-18}$ cm^3/ns and the trap parameter is $\alpha = 0.09\ \mu$eV μm^{-2}.

The result for the temperature using a pump power of $P_L = 3\ \mu$W is shown in the left panel of Fig. 4. It first falls to a minimum of $T_{min} = 0.23$ K at $r = 10\ \mu$m and reaches a local maximum in the trap center with $T_0 = 0.25$ K. The mean temperature is $\langle T \rangle = 0.40$ K and hence very close to the experimentally determined spectral temperature of $T_S = 0.41$ K (compare Fig. 3 of Ref. [18]). The experimentally determined exciton number was $N_{Expt} = 2.6 \times 10^6$ which agrees well with the value of $N = 2.78 \times 10^6$ predicted by our model. In the right panel of Fig. 4 we compare the experimentally determined exciton numbers and spectral temperatures T_S with the corresponding theoretical results for exciton number and mean temperature $\langle T \rangle$ over a wide range of pumping powers. As before, the quantities agree well with the experimental values. This suggests to identify the spectral temperature T_S from the experiments with the mean temperature of the excitons $\langle T \rangle$, which seems intuitively plausible. If this is correct, the spectral temperature is actually considerably higher than the temperature of the excitons in the trap center (see Fig. 4). This was already proposed in Ref. [18] to explain some of the experimental features and is consistent with the typical results discussed in the previous section. To further substantiate the identification $T_S = \langle T \rangle$ one would need to calculate the spectrum and apply the same fitting procedure as in the experiments. For this a theory of luminescence for interacting excitons in an inhomogeneous system in a nonequilibrium state is needed. To our knowledge, there is no fully developed theory for this purpose at the moment. This is an open problem that needs to be solved in the future.

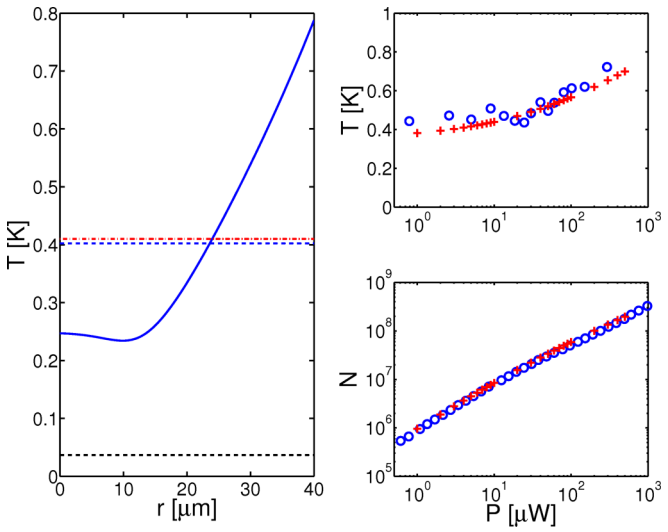

FIG. 4. (Color online) Left panel: Exciton temperature $T(r)$ (solid blue curve) and the mean exciton temperature $\langle T \rangle = 0.40$ K (dashed blue curve) under cw excitation with a pump power of $P_L = 3\ \mu$W and a phonon temperature of $T_{Ph} = 0.037$ K (dashed black curve) in the stationary state. The dashed red curve shows the experimentally determined spectral temperature $T_S = 0.41$ K (compare Fig. 3 in Ref. [18]). Right panel: Experimentally determined exciton numbers and spectral temperatures T_S (blue circles) for different pump powers (compare Fig. 11 in Ref. [18]) in comparison with the exciton numbers and the mean temperatures $\langle T \rangle$ (red crosses) as predicted by our theory.

The second set of experimental data is taken from Ref. [16], Figs. 8 and 9. Using pulsed excitation, the exciton number and the spectral temperature T_S were experimentally determined for a bath temperature of $T_B = 0.82$ K. For the calculations we used $\alpha = 0.11\ \mu$eV μm^{-2} and $A = 2.0 \times 10^{-18}$ cm^3/ns. The theoretical results for the mean temperature and the exciton number as well as their experimental counterparts are shown in Fig. 5. The calculated exciton numbers agree well with the experimental results. Only the second and third value show stronger discrepancies. The reason for this is probably the neglection of the orthoexcitons in our calculations. In the experiments, the orthoexcitons create new paraexcitons by conversion even when the laser is switched off. In the present form of the theoretical model this effect is not included.

The calculated mean temperature $\langle T \rangle$ and the experimentally determined spectral temperature T_S do not agree. The

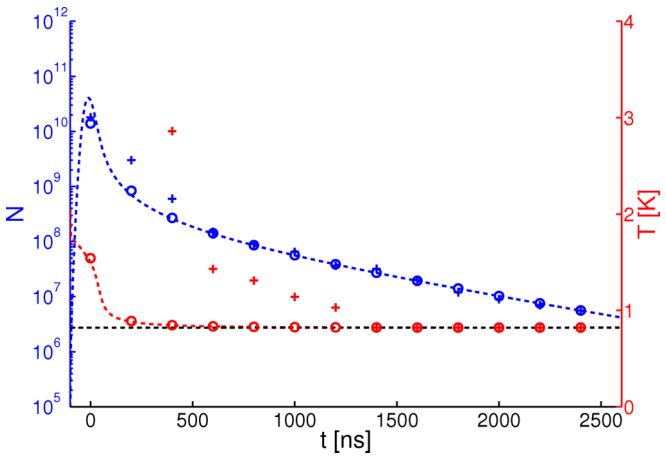

FIG. 5. (Color online) Calculated exciton number $N(t)$ (dashed blue line) and mean temperature $\langle T \rangle$ (dashed red line) under pulsed excitation for a phonon temperature of $T_{Ph} = 0.82$ K. The laser pulse has been modeled according to the data provided in Ref. [16]. The blue and red circles represent the theoretical values averaged over a gate width of 200 ns. The blue and red crosses represent the experimentally determined values with the same gate width [16]. The Auger rate is set to $A = 2.0 \times 10^{-18}$ cm^3/ns.

first two points of the spectral temperature are even off the scale (the values are 12.5 and 6.0 K). According to the theory presented here and in Ref. [28], temperatures around 4 K should be reached in less than 1 ns. However, in this case, the experimentally determined spectral temperature T_S is 6.0 K after 400 ns. Since the parameters and the collision term for the X-Ph interaction are well known, we exclude both as origin of the discrepancy. An increased Auger rate can also not explain the differences since the newly formed excitons cool rapidly to temperatures around 4 K. The most probable explanation for the differences is a heating of the specimen by the pump laser and, therefore, $T_{Ph} > T_B$. As a result, the excitons cool only to the respective lattice temperature, which is higher than the temperature of the surrounding helium bath. Once the laser is turned off, the crystal slowly cools down to the bath temperature and the excitons with it. Therefore, it is very likely that the temperature curves in Ref. [16] actually show the cooling process of the crystal rather than that of the excitons.

VI. CONCLUSION AND OUTLOOK

In this paper we developed a theoretical model to describe trapped ultracold paraexcitons in Cu_2O out of equilibrium. It uses a generalized Gross-Pitaevskii equation for describing a possible condensate and a set of hydrodynamic equations for the thermal excitons. The finite lifetime, the Auger-like two-body decay, the pump laser, exciton-exciton, and exciton-phonon interaction have been taken into account.

The numerical results obtained using continuous wave excitation revealed some important features of the stationary states of the excitonic system. First of all, the stationary states are true nonequilibrium situations which cannot be approximated using a global equilibrium distribution. Second, the excitons do not fully thermalize with the crystal lattice at ultralow temperatures ($T_{Ph} \ll 1.0$ K). There is a distinct gap between the actual exciton and the respective phonon temperature which continuously increases for sinking phonon temperatures. This is due to the long thermalization time and the Auger effect. The latter strongly influences the exciton densities and temperatures for high pumping powers and at ultralow temperatures.

Comparing the exciton numbers predicted by our model with experimental results for pulsed and continuous wave excitation yields reasonable agreement. Furthermore, comparing the mean temperature $\langle T \rangle$ from the calculations with the experimentally determined spectral temperatures T_S under continuous wave excitation suggests the identification $\langle T \rangle = T_S$. As a result, the excitons in the trap center are actually cooler than the spectral temperature suggests. This preposition was already made in a previous paper [18] to explain some of the experimental features. However, comparing the experimentally determined and theoretically predicted temperatures under pulsed excitation showed strong discrepancies between the two. The most probable explanation for this is a heating of the crystal. If that is the case then the experimentally determined evolution of the spectral temperature is closely related to the cooling process of the crystal lattice rather than that of the excitons. It is well known that high pump powers can lead to heating of the specimen and even of the surrounding helium bath. In principle, the temperature of the crystal lattice can be determined using Brillouin scattering. However, this is very difficult experimentally and, to our knowledge, has not been done yet. If our interpretation of the experimental data is correct, experiments under pulsed excitation with varying pump powers might be an opportunity to study the cooling process of the crystal lattice indirectly in a simple fashion.

In conclusion, the theoretical results obtained by our model are intuitively plausible and yield reasonable agreement with the exciton numbers and spectral temperatures obtained experimentally. The results presented in this paper are, therefore, an important step to improve the understanding of the experiments. Unfortunately, there are still some crucial problems that need to be addressed. Most importantly, the theoretical model must be able to reliably predict parameters for the onset of Bose-Einstein condensation (i.e., the vanishing of the effective chemical potential). However, within the present model, a quantitative discussion of the condensation parameters would not yield reliable results mainly due to the uncertainties associated with the Auger decay. Since the Auger effect reduces the density while increasing the temperature, its modeling and the parameters associated with it are of paramount importance for predicting the condensation threshold. However, the Auger rates A reported in the literature by different authors vary over 6 orders of magnitude. Additionally, to our knowledge, there are no theoretical results that agree with any of the experimentally determined Auger rates. Furthermore, using a $\mathbf{k}$-averaged constant A as Auger rate is itself already a simplification. According to the theoretical works on the Auger decay [32], the rate A should be proportional to some power of k. Using such a k-dependent rate would primarily destroy high energy excitons, while affecting low energy excitons much less. An inclusion of such a k-dependent Auger rate will have strong effects on the parameters for condensation. Moreover, in a strain free crystal of Cu_2O, the Auger decay of the paraexcitons under consideration is negligible [32]. The experimentally observed Auger decay of these excitons is due to the ortho-para Auger decay and the effects the applied stress has on the exciton states. The former can only be included by modeling a multicomponent system of para- and orthoexcitons. Therefore, considering these uncertainties, we refrain from a discussion of the condensation threshold at this point. In order to make reliable predictions for the onset of Bose-Einstein condensation, the problems discussed above have to be addressed first.

Another important extension to the theoretical model is using a symmetry which fits the experimental geometry better, i.e., cylindrical (quasi-two-dimensional) instead of spherical (quasi-one-dimensional). This should yield more realistic theoretical results. More importantly though, in order to directly compare the theoretical and experimental results, we need to be able to calculate the luminescence spectrum of the excitons. Being able to differentiate between the spectra of excitons in quasiequilibrium, a stationary state, or a condensed case is crucial. It is especially important to identify unique spectral features of a condensate like it was already done for excitons in equilibrium [39,40]. This requires us to develop a

theory of excitonic luminescence for inhomogeneous systems in nonequilibrium. One possible approach is to start from the first order correlation function [41] treating the photons by an equation of motion method [42,43]. This is work in progress and will be the subject of a future publication.

ACKNOWLEDGMENTS

We would like to thank G. Manzke, W.-D. Kraeft, Th. Bornath, Th. Koch, and H. Fehske for many fruitful discussions. This work was supported by the Deutsche Forschungsgemeinschaft via Collaborative Research Center SFB 652.

[1] S. A. Moskalenko, Fiz. Tverd. Tela **4**, 276 (1962) [Sov. Phys.-Solid State **4**, 199 (1962)].
[2] I. M. Blatt, K. W. Boer, and W. Brandt, Phys. Rev. **126**, 1691 (1962).
[3] H. Kuroda, S. Shionoya, H. Saito, and E. Hanamura, Solid State Commun. **12**, 533 (1973).
[4] H. Deng, G. Weihs, C. Santori, J. Bloch, and Y. Yamamoto, Science **298**, 199 (2002).
[5] J. Kasprzak, M. Richard, S. Kundermann, A. Baas, P. Jeambrun, J. M. J. Keeling, F. M. Marchetti, M. H. Szymańska, R. André, J. L. Staehli, V. Savona, P. B. Littlewood, B. Deveaud, and L. S. Dang, Nature (London) **443**, 409 (2006).
[6] R. B. Balili, V. Hartwell, D. Snoke, L. Pfeiffer, and K. West, Science **316**, 1007 (2007).
[7] H. Deng, H. Haug, and Y. Yamamoto, Rev. Mod. Phys. **82**, 1489 (2010).
[8] Z. Vörös, D. W. Snoke, L. Pfeiffer, and K. West, Phys. Rev. Lett. **97**, 016803 (2006).
[9] A. A. High, J. R. Leonard, M. Remeika, L. V. Butov, M. Hanson, and A. C. Gossard, Nano Lett. **12**, 2605 (2012).
[10] G. J. Schinner, J. Repp, E. Schubert, A. K. Rai, D. Reuter, A. D. Wieck, A. O. Govorov, A. W. Holleitner, and J. P. Kotthaus, Phys. Rev. B **87**, 205302 (2013).
[11] D. Semkat, S. Sobkowiak, G. Manzke, and H. Stolz, Nano Lett. **12**, 5055 (2012).
[12] D. W. Snoke, J. P. Wolfe, and A. Mysyrowicz, Phys. Rev. Lett. **64**, 2543 (1990).
[13] J. L. Lin and J. P. Wolfe, Phys. Rev. Lett. **71**, 1222 (1993).
[14] D. Snoke, Science **298**, 1368 (2002).
[15] K. Yoshioka, E. Chae, and M. Kuwata-Gonokami, Nat. Commun. **2**, 328 (2011).
[16] R. Schwartz, N. Naka, F. Kieseling, and H. Stolz, New J. Phys. **14**, 023054 (2012).
[17] D. W. Snoke, Phys. Status Solidi B **238**, 389 (2003).
[18] H. Stolz, R. Schwartz, F. Kieseling, S. Som, M. Kaupsch, S. Sobkowiak, D. Semkat, N. Naka, Th. Koch, and H. Fehske, New J. Phys. **14**, 105007 (2012).
[19] K. Yoshioka, Y. Morita, K. Fukuoka, and M. Kuwata-Gonokami, Phys. Rev. B **88**, 041201 (2013).
[20] A. L. Ivanov, C. Ell, and H. Haug, Phys. Rev. E **55**, 6363 (1997).
[21] D. W. Snoke and J. P. Wolfe, Phys. Rev. B **39**, 4030 (1989).
[22] K. E. O'Hara and J. P. Wolfe, Phys. Rev. B **62**, 12909 (2000).
[23] S. Denev and D. W. Snoke, Phys. Rev. B **65**, 085211 (2002).
[24] N. P. Proukakis and B. Jackson, J. Phys. B **41**, 203002 (2008).
[25] A. Griffin, T. Nikuni, and E. Zaremba, *Bose-Condensed Gases at Finite Temperatures* (Cambridge University Press, Cambridge, 2009).
[26] E. Zaremba, T. Nikuni, and A. Griffin, J. Low Temp. Phys. **116**, 277 (1999).
[27] M. Imamovic-Tomasovic and A. Griffin, J. Low Temp. Phys. **122**, 617 (2001).
[28] S. Sobkowiak, D. Semkat, and H. Stolz, Phys. Rev. B **90**, 075206 (2014).
[29] H. Haug, T. D. Doan, and D. B. Tran Thoai, Phys. Rev. B **89**, 155302 (2014).
[30] D. P. Trauernicht and J. P. Wolfe, Phys. Rev. B **33**, 8506 (1986).
[31] K. Reimann and K. Syassen, Phys. Rev. B **39**, 11113 (1989).
[32] G. M. Kavoulakis and G. Baym, Phys. Rev. B **54**, 16625 (1996).
[33] K. E. O'Hara, J. R. Gullingsrud, and J. P. Wolfe, Phys. Rev. B **60**, 10872 (1999).
[34] K. Yoshioka, T. Ideguchi, A. Mysyrowicz, and M. Kuwata-Gonokami, Phys. Rev. B **82**, 041201 (2010).
[35] J. I. Jang and J. P. Wolfe, Solid State Commun. **137**, 91 (2006).
[36] M. Wouters and V. Savona, Phys. Rev. B **79**, 165302 (2009).
[37] J. Shumway and D. M. Ceperley, Phys. Rev. B **63**, 165209 (2001).
[38] J. Brandt, D. Fröhlich, C. Sandfort, M. Bayer, H. Stolz, and N. Naka, Phys. Rev. Lett. **99**, 217403 (2007).
[39] S. Sobkowiak, D. Semkat, H. Stolz, Th. Koch, and H. Fehske, Phys. Rev. B **82**, 064505 (2010).
[40] S. Sobkowiak, D. Semkat, H. Stolz, Th. Koch, and H. Fehske, Phys. Status Solidi C **8**, 1178 (2011).
[41] R. J. Glauber, Phys. Rev. **130**, 2529 (1963).
[42] H. Stolz, *Time-Resolved Light Scattering from Excitons*, Springer Tracts in Modern Physics, Vol. 130 (Springer, Berlin, 1994).
[43] B. Laikhtman, Europhys. Lett. **43**, 53 (1998).